SENRA Academic Publishers, Burnaby, British Columbia
Vol. 2, No. 1, pp. 197-203, 2008
ISSN: 1715-9997

Canadian Journal of pure&applied sciences

FINITE ELEMENT SIMULATION OF CARDIAC OUTPUT AND PRESSURE WAVEFORM IN CAROTID ARTERY

Ruchi Agarwal[2] , *VK Katiyar[1], Prabhakar Pradhan[2] and D Liepsch[3]
Department of Mathematics, [1]Indian Institute of Technology, Roorkee, India
[2]Gurukul Kangari University, Haridwar, India
[3] Fachhochschule München, Germany

ABSTRACT

Cerebral transient ischemic attacks and strokes are usually related to embolic occlusion of cerebral arteries, which originates from the heart. It causes due to the hemodynamic impact of cardiac function on the flow in the brain-supplying arteries, i.e., carotid arteries. The ischemic attacks and strokes can be minimized by increasing cardiac output and reducing the resistance which decreases the arterial pressure. The nonlinear unsteady flow phenomenon is governed by the Navier-Stokes equations. These equations with appropriate boundary conditions describe the present biomechanical problem and are solved numerically by adopting finite element technique. The respective profiles of the cardiac output, flow rate, arterial pressure and flow velocity in terms of pressure waveform as well are obtained. The obtained results are compared with the available experimental observations.

Keywords: Carotid artery, pressure waveform, cardiac output, FEM, ANSYS.

INTRODUCTION

Nearly 75% of all deaths in the western world are caused due to circulatory diseases. Of these, atherosclerosis is the most frequent, usually found at bends and bifurcations of human arteries. Flow of blood through such bifurcations is not simple, due to complex geometry of the branching, the pulsatile nature of the flow, the distensibility of the arterial wall and the non-Newtonian characteristics of the blood. Thus, due to clinical importance of carotid artery bifurcation detailed knowledge of it must be necessary. The common carotid artery divides into the external and the internal. The internal carotid artery generally shows a widening in its proximal part called carotid sinus. A large range of flow separation was found along the outer wall of the carotid sinus and wall shear stress was very low in magnitude.

Different studies have shown that atherosclerotic sites correlate strongly with the regions of disturbed flow Ku (1997). The influence of both vessel wall elasticity and peripheral resistance on the flow wave form was obtained from a CFD simulation of blood flow in the carotid artery bifurcation Perktold and Hilbert (1985), Perktold *et al.* (1994) and Maurits *et al.* (2007). Pulsatile flow in carotid artery bifurcation was studied showing a coupling effect between fluid flow and elastic deformation Liepsch and Zimmer (1995) and Agarwal *et al.* (2006). In last few decades Computational Fluid Dynamics (CFD) studies have greatly enlarged our knowledge of hemodynamic factors involved in atherogenesis Quarteroni *et al.* (2000) and Stroud *et al.* (2002). Different CFD results have been directly compared to hemodynamic flow parameters obtained in vivo Bharadvaj *et al.* (1982); Liepsch *et al.* (1992), Ku and Giddens (1987) and Zhao *et al.* (2000). Even in healthy subjects, the waveforms in the common (CCA), internal (ICA) and external (ECA) carotid artery have different shapes, due to higher wall shear stress in the arteries and decreasing elasticity with distance from the bifurcation in the ICA and ECA branches compared to the CCA Marshall *et al.* (2004).

Recently, the coupling and integration of models with different dimensionality have been analyzed, linking together lumped models with 3-D models of the arterial tree Rindt *et al.* (1990), Van de Vosse *et al.* (1990), Baaijens *et al.* (1993), Formaggia *et al.* (2001) and Urquiza *et al.* (2006). Three different outflow treatment schemes, showing the variation of flow patterns strongly influenced by outflow conditions have been compared Augst *et al.* (2003) and Clementel *et al.* (2006). However, wall movement was neglected in the latter study. The impact of cardiac output on cerebral perfusion is controversial. The increase of cardiac output does not increase cerebral blood flow however a drop in cardiac output led to a corresponding cerebral blood flow reduction Castello *et al.* (1995), Stevens *et al.* (2003) and Eicke *et al.* (2001).

The objective of this paper is to investigate the influence of cardiac output in the carotid artery. Keeping in view the motivation stated above, a sincere attempt is made to formulate an unsteady two dimensional carotid artery numerically in the present investigation in order to estimate some important characteristic of blood flow. The flowing of blood contained in the carotid artery is

*Corresponding author email: ruchiiitr83@gmail.com, vktmafma@rediffmail.com

considered to be Newtonian. The cylindrical coordinate system has been taken for analytical formulation. The unsteady non-linear Navier-Stokes equations of motion governing blood flow coupled to the velocity field are taken up along with the appropriate initial and boundary conditions in order to define the present biomechanical problem. The equations are solved numerically by employing a suitable finite element method (FEM) with the use of boundary and matching conditions in concert with the physical representation of the problem. A thorough qualitative analysis has finally been performed at the end of the paper through graphical representations of the results together with their discussion at length in order to validate the applicability of the present mathematical model.

Mathematical model

Geometrical model and flow conditions

It is known that essential variations occur in the anatomy of the human carotid artery bifurcation. Based on data from literature, a 2-D model of the carotid artery bifurcation is considered. The geometry of the normal carotid artery bifurcation was derived from the available literature Bharadvaj *et al*. (1982). The bifurcation model of carotid artery and

The lines L20, L21, L24 and L27 in fig.1 indicate different flow cross-sections where numerical results are presented. The inlet diameter of common carotid artery (CCA) is $D = 8mm$ and near bifurcation diameter is $D = 9mm$. The internal and external outlet diameters are $D = 5.5mm$ and $D = 4.1mm$ respectively. The mid-sinus diameter of internal carotid artery (ICA) is $D = 9.5mm$. The angle between the CCA and ICA is $22°$ and between the CCA and ECA is $33°$ for a total angle of $52°$ between the internal and external carotid artery.

Calculations are carried out under constant pulsatile flow conditions. The pulse wave frequency is 1.045 Hz, which is equivalent to 72 beats per minute. The mean flow rate in the common carotid is assumed to be $400ml/\min$. A time and space-averaged mean inflow velocity of $u_0 = 0.145m/s$ was used. The ratio of flow divided between the internal carotid and external carotid was assumed to be 70-30%, thus the mean flow rate is $280ml/\min$ and $120ml/\min$ in the internal and the external carotid, respectively. The mean Reynolds number amounts to about 250 and varies from about 175 to 650, so laminar flow can be assumed. If furthermore a cardiac cycle time of 1s is assumed, the frequency parameter or Womersley number $\alpha = 4.3$. A Kinematic viscosity $\upsilon = 4\times10^{-6}m^2/s$ and a mass density $\rho = 1050kg/m^3$ were kept constant.

Governing equations

Blood flow in the artery is considered to be incompressible and Newtonian, consisting of the unsteady 2-D continuity and Navier-Stokes equations in cylindrical coordinate system. For convenience, the model is described using cylindrical polar coordinates r,θ,z with the axis of *z* lying along the central axis of the vessel and $z = 0$ at the entrance of the vessel. The problem is independent of θ due to symmetry. The governing equations are written as follows,

$$\frac{1}{r}\frac{\partial}{\partial r}(ru_r) + \frac{\partial u_z}{\partial z} = 0 \quad (1)$$

$$\frac{\partial u_r}{\partial t} + u_r\frac{\partial u_r}{\partial r} + u_z\frac{\partial u_r}{\partial z} = -\frac{\partial p}{\partial r} + \frac{1}{\mathrm{Re}}\left(\frac{\partial^2 u_r}{\partial z^2} + \frac{\partial^2 u_r}{\partial r^2} + \frac{1}{r}\frac{\partial u_r}{\partial r} - \frac{u_r}{r^2}\right) \quad (2)$$

$$\frac{\partial u_z}{\partial t} + u_r\frac{\partial u_z}{\partial r} + u_z\frac{\partial u_z}{\partial z} = -\frac{\partial p}{\partial z} + \frac{1}{\mathrm{Re}}\left(\frac{\partial^2 u_z}{\partial z^2} + \frac{\partial^2 u_z}{\partial r^2} + \frac{1}{r}\frac{\partial u_z}{\partial r}\right) \quad (3)$$

where the following non-dimensional variables were used,

$$u_r = \frac{\bar{u}_r}{u_0};\ u_z = \frac{\bar{u}_z}{u_0};\ p = \frac{\bar{p}}{\rho {u_0}^2};\ z = \frac{\bar{z}}{R_0};$$

$$r = \frac{\bar{r}}{R_0};\ t = \frac{\bar{t}u_0}{R_0} \quad (4)$$

here u_r, u_z represents the radial and the axial velocity, p the pressure, ρ the density, μ the viscosity of the blood and u_0 is the time-averaged reference velocity at the inlet.

The dimensionless group used represents,

- $\mathrm{Re} = \frac{\rho u_0 R_0}{\mu}$, the Reynolds number of the flow.
- $\alpha = R\sqrt{\omega/\upsilon}$, the Womersley number ($\upsilon$ is the Kinematic viscosity of blood, $\omega = 2\pi f\ (= 2\pi/T)$ is the angular frequency.

Now the volumetric flow rate of the fluid at *r*=*R* can be defined as,

$$Q = \int_0^R 2\pi r u_z dr \quad (5)$$

and also the cardiac output is given by,

$$CO = \int_0^T Q dt \quad (6)$$

where, T is the time period for one cardiac-cycle.

2.3. Boundary conditions

Since the actual blood flow in the artery is pulsatile, pulsatile boundary condition is prescribed on the inflow boundary. The solution of equations (1)-(3) is assumed to satisfy appropriate boundary conditions. Due to the lack of experimental data for the shape of the time-dependent

inflow velocity profiles as well as for outflow conditions, appropriate mathematical functions must be applied to simulate the physiological conditions. At the inflow boundary, fully developed time-dependent velocity profiles are applied as given in equation (7). These profiles we calculated as long straight tube profiles for the velocity waveform. The assumption of fully developed flow at the entrance to the bifurcation agrees with literature Ku and Giddens (1987).

$$u_z = u_0\left[1-\left(\frac{r_z}{R}\right)^2\right], \quad u_r = 0 \tag{7}$$

where r_z is the distance from the origin.

At the walls non-slip condition is imposed,

$$u_r = 0\,, \quad u_z = 0 \tag{8}$$

A zero-surface traction is applied to outflow boundary conditions Perktold and Hilbert (1985). This condition is modeled mathematically as,

$$-pn + \frac{1}{\mathrm{Re}}\frac{\partial u}{\partial n} = 0 \tag{9}$$

where $n = (n_r, n_z)^T$ and $u = (u_r, u_z)$ denotes the unit normal vector at the outflow boundary. This equation is not the

In bifurcation flow two outflow boundaries appear. From the assumed flow division ratio, the condition describing surface forces cannot be applied directly at both outflow boundaries. Here at the external outflow boundary, an appropriate time-dependent velocity profile calculated in a pre-processor step is used, where as at the internal outflow boundary, equation (7) is applied. Thus, the pressure at the outlets prescribed as these constants

$p = 0Pa$ (at external),

$p = 5.2Pa$ (at internal) (10)

Numerical approach

Equation (1)-(3) with the proper boundary conditions stated above were solved by means of the Finite Element Method (FEM) using ANSYS Multiphysics Version 10.0, finite element solver package the 3-D cylindrical geometry of carotid artery is modeled as a 2-D geometry. The model was created in the software and was meshed with its mesh generator with FLUID141 element. The model is meshed automatically using ANSYS 'mesh tool'. The mesh is created using 'mapped meshing' instead of 'free meshing' (Fig. 2). Mapped meshing is used when only quadrilateral (or triangular) elements are required. The meshing is specified as mapped when the command MSHKEY is set to 1. Smart sizing cannot be used for mapped meshing. For an area to accept a mapped mesh, the area must be bounded by either 3 or 4 lines (with or without concatenation). In order to achieve this in case near bifurcation, which is bounded by 6 lines in the model, the lines L15, L16, L19, L24, L25 and L26 (Fig.1) were concatenated to form a single line. The grid had maximum 1660 elements with 1801 corner nodes. The loads (boundary conditions) are then applied. One pulse cycle was discretized into 100 time steps. The solution was obtained by a finite element method, and SIMPLEF was chosen for solution algorithm with desecrates the momentum equations with a Streamline Upwind/Petrov-Galerkin (SUPG) approach.

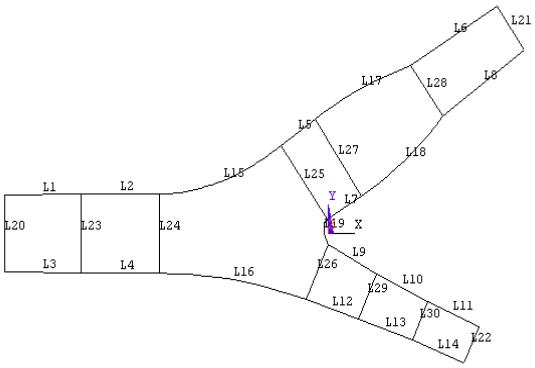

Fig.1. Geometry of two-dimensional model of carotid artery bifurcation.

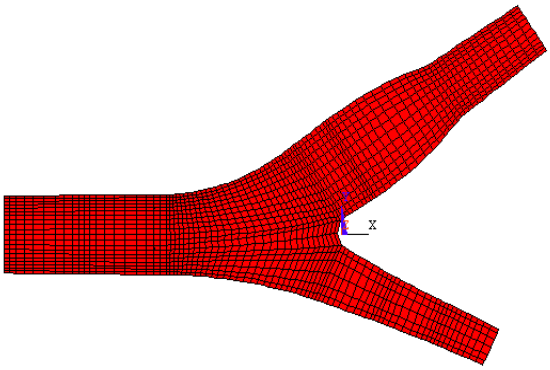

Fig. 2. Mesh generation of two-dimensional model of carotid artery bifurcation.

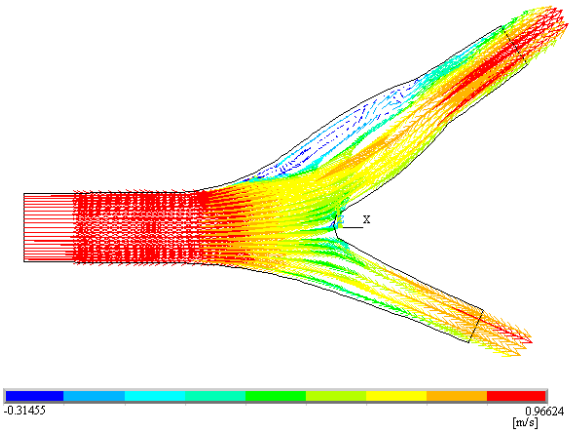

Fig. 3. The vector plot of velocity field in carotid artery over one cardiac cycle.

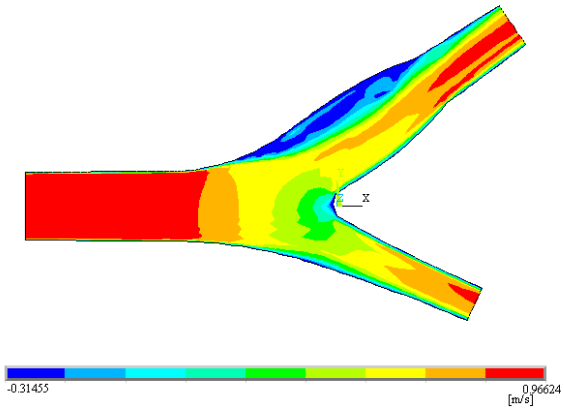

Fig. 4. The color contours describing the velocity distribution over one cardiac cycle.

RESULTS AND DISCUSSIONS

At first calculation flow rate at the inlet of common carotid artery was selected $275ml/\min$ and the Reynolds number $\mathrm{Re} = 250$. Fig. 3 and 4 shows the velocity vector and contour field in the branching plane at the time of systolic acceleration. The flow separation occurs near the outer wall of the ICA in sinus. In this region flow recirculation occurred and pressure decreases. Fig. 5 shows the total stagnation pressure in carotid artery at systolic acceleration. The pressure decreases near the outer wall of carotid sinus.

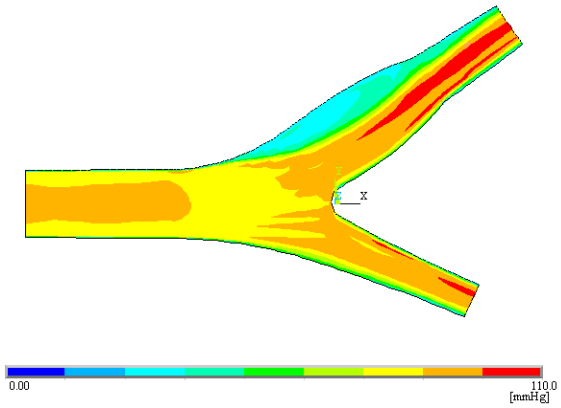

Fig. 5. Distribution of total stagnation pressure over one cardiac cycle in carotid artery.

Velocity profile

The axial velocity profiles were determined for $t = 0.00s$ (end diastole), $t = 0.08s$ (peak systole), $t = 0.16s$ (halfway systolic deceleration) and $t = 0.32s$ (end systole) respectively. These axial velocities were calculated at four different cross-sections, i.e., at inlet, near bifurcation, in carotid sinus and at outlet of ICA. During inlet (Fig. 6) the axial velocity profile is almost parabolic at the end of diastolic phase ($t = 0.00s$). Then the velocity rapidly increases during systolic acceleration ($t = 0.08s$) resulting in a slight flattening of the profile. During the systolic deceleration ($t = 0.16s$) the profile show a tendency to flow reversal at both walls and finally develops a parabolic shape at the end of the systolic phase ($t = 0.32s$) of the flow. Axial velocity profile near the bifurcation (Fig. 7) during the end diastole ($t = 0.00s$) is almost parabolic similar to the profile at inlet. But during the peak systole ($t = 0.08s$) the velocity profile becomes blunt shaped as the flow separation occurs at the apex. Again during the systolic deceleration ($t = 0.16s$) and end systole ($t = 0.32s$) the velocity profile retains the parabolic shape due to flow reversal at both walls.

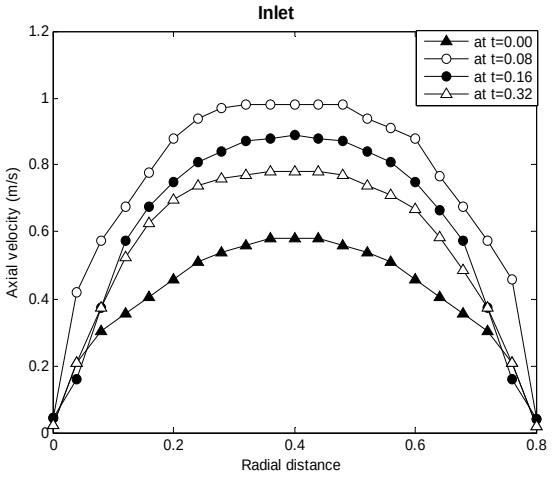

Fig. 6. Velocity profile at the inlet in CCA for different values of time.

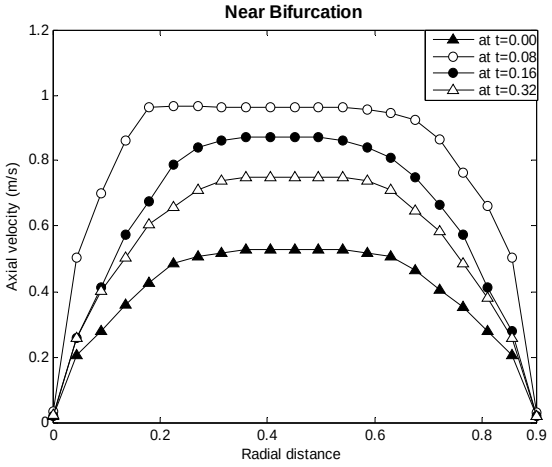

Fig.7. Velocity profile near the bifurcation in CCA for different values of times.

A small local maximum is observed in the most distal part of the sinus where the walls converge maximally and develop into the parallel wall section of the internal carotid artery. During systolic deceleration ($t = 0.16s$) large differences in the axial velocities are found in the carotid sinus (Fig. 8). Relatively large negative velocities

are found at the non-divider side wall downstream the apex. The region of reversed flow occupies up to 30% of the local diameter and is associated with high positive velocities at the divider side wall where a large peak is found. Downstream of the carotid sinus the profile gradually recovers a parabolic shape. Near the end of the systolic deceleration phase ($t = 0.32s$), the axial velocity profile in the carotid sinus becomes more complicated. At the mid-sinus, the axial velocity profile is characterized by a relatively large region with small negative velocities at the non-divider side wall, similar to the pattern at end diastolic flow ($t = 0.00s$). During peak systole ($t = 0.08s$) the profile has very small negative velocities for a relatively small region. The axial velocity profiles at the outlet of internal carotid artery are similar to the pattern at the inlet of common carotid artery (Fig. 9) but have small values of velocity.

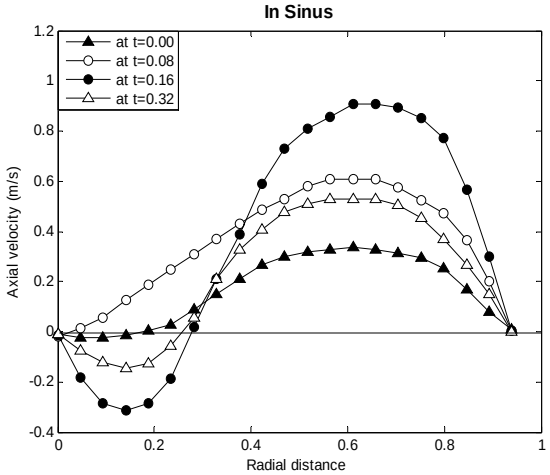

Fig. 8. Velocity profile in the carotid artery sinus for different values of time.

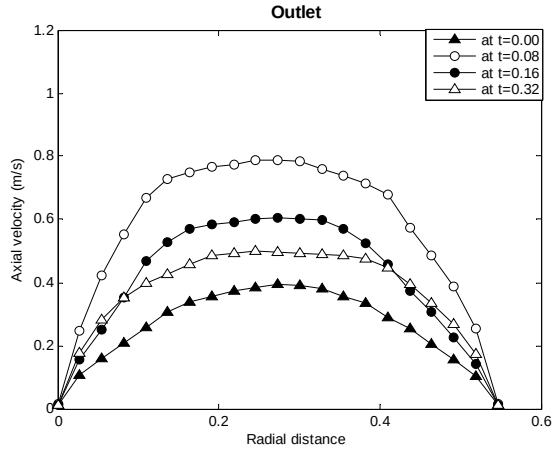

Fig. 9. Velocity profile at the outlet in ICA for different values of time.

Flow and pressure curves

With the aim of examining the consistency of the model, flow and pressure curves are analyzed. The results are plotted at the inlet of common carotid artery and outlet of internal carotid artery during whole cardiac cycle of 1s. On analysis of the pressure generated we saw that the pattern of calculated pressure curve (Fig. 10 and 11) is of the form of the normal pressure curve Clementel *et al.* (2006) and Urquiza *et al.* (2006). There is not so much difference in the inlet and outlet pressure curves. The peak value of pressure at inlet is $110mmHg$ and outlet is $109.5mmHg$ during $t = 0.2s$. The pressure distribution (Fig. 5) illustrated that in the common carotid artery, the pressure along axis in common carotid first decreases according to a straight line. When the non-divider wall of artery changes from a straight to a curved line (carotid sinus), the pressure reaches its minimum. After this minimum, the pressure increases slightly in the ICA. The flow rate curve (Fig. 10 and 11), during inlet and outlet are of same pattern but at inlet the pressure lags the inflow rate. The peak flow during inlet is $35ml/s$ and during outlet is $19ml/s$ at $t = 0.1s$. The negative values of flow are due to the existence of reversal flow. The minimum value at inlet is $12ml/s$ and outlet is $7ml/s$. Thus, the flow rate is maximum during the inlet.

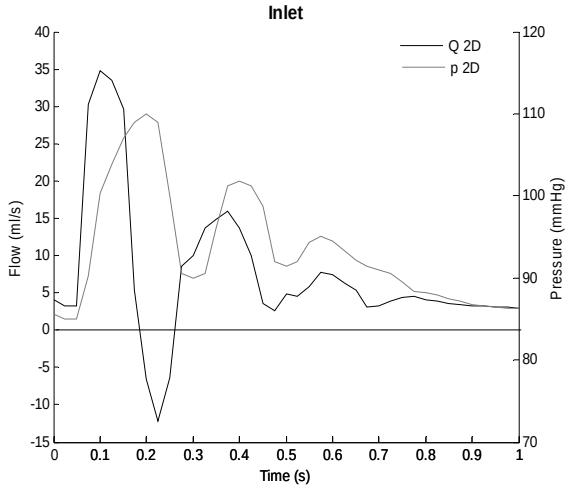

Fig. 10. Flow rate and pressure curves at the inlet of carotid artery.

Cardiac output

The mean heart rate was 72 beats per minute. The averaged total blood flow volume (TBFV) is $228ml/\min$. The total blood flow volume (TBFV) and cardiac output in carotid artery does not show any correlation numerically Castello *et al.* (1995) and Eicke *et al.* (2001). As the increase in blood flow did not show any increase in cardiac output, however, a drop in cardiac output led to a corresponding reduction in blood flow (Fig. 12). The cardiac output shows a negative but significant correlation with the arterial pressure (Fig. 13).

As the arterial pressure decreases, the cardiac output increases. The mean arterial pressure was found to be $94 mmHg$.

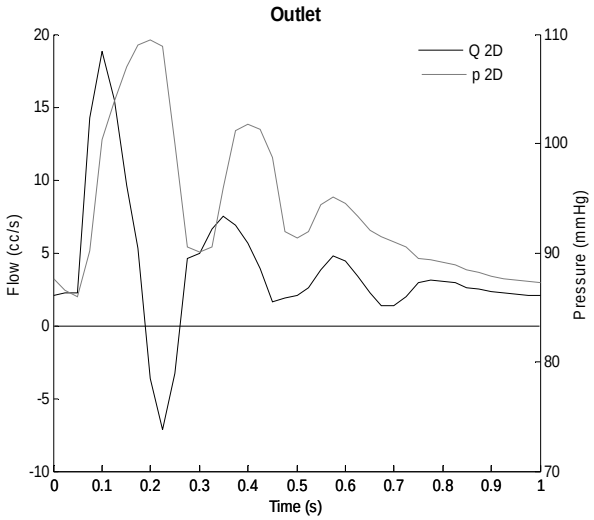

Fig. 11. Flow rate and pressure curves at the major outlet (ICA) of carotid artery.

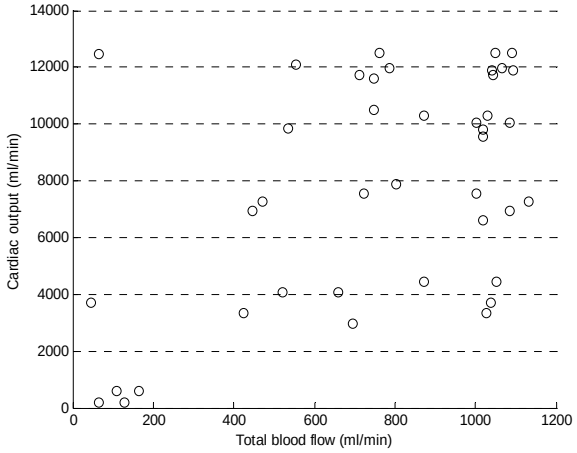

Fig. 12. Scattergram of cardiac output and total blood flow showing lack of correlation.

CONCLUSION

In our paper, we have numerically discussed velocity profile, pressure and flow waveforms and influence of cardiac output. The study was carried out in 2-D model of carotid artery assuming the flow to be unsteady. Based on our analysis the following can be concluded:

- The velocity profile shows major changes near bifurcation (at apex) and at the non-divider wall. Large negative velocities are found in the sinus region giving the largest recirculation zone.
- The height of pressure peaks decreases with increase in time. The pressure is very low in the recirculation zone.
- The flow is influenced by the flow divider and widening & tapering of the sinus. This widening features flow reversal at the end diastolic flow rate.
- The impact of cardiac output on cerebral perfusion is controversial. Increase in blood flow does not increase cardiac output whereas a drop in cardiac output decreases the blood flow in carotid artery.
- Cardiac output and arterial pressure shows a significant but negative correlation. A decrease in arterial pressure shows an increase in cardiac output.

This problem has a clinical importance as the decrease in cardiac output can cause the attacks and strokes. The results we obtained numerically shows close resemblance with the experimental data available. By using the more realistic conditions in the computations we believe that the measurements of the parameters can be improved.

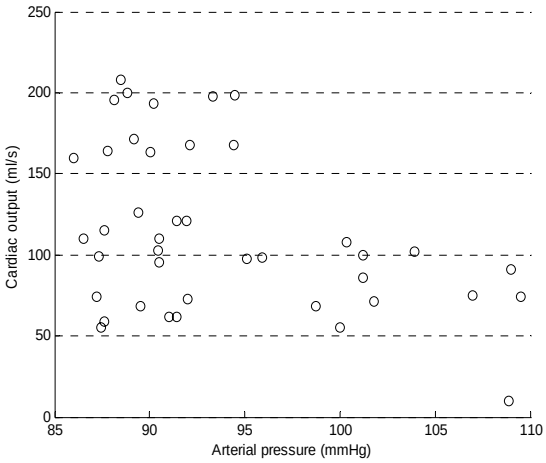

Fig. 13. Scattergram of cardiac output and arterial pressure showing negative but significant correlation.

REFERENCES

Agarwal, R., Katiyar, VK. and Pradhan, P. 2006. Pulsatile flow in carotid artery bifurcation. Journal of Biomechanics. 39(supplement 1): S321.

Augst, AD., Barrat, DC., Hughes, AD., Thom, SAM. and Xu, XY. 2003. Various issues relating to computational fluid dynamics simulations of carotid bifurcation flow based on model reconstructed from three-dimensional ultrasound images. Proceedings of The Institution of Mechanical Engineers Part H-Journal of Engineering in Medicine. 217: 393-403.

Baaijens, JPW., Steenhoven, AAV. and Janssen, JD. 1993. Numerical Analysis of Steady Generalized Newtonian Blood flow in a 2D-Model of the Carotid Artery Bifurcation. Biorheology. 30: 63-74.

Bharadvaj, BK., Mabon, RF. and Giddens, DP. 1982. Steady flow in a model of the human carotid bifurcation. Part I – Flow visualization. Journal of Biomechanics. 15**:** 349-362.

Bharadvaj, BK., Mabon, RF. and Giddens, DP. 1982. Steady flow in a model of the human carotid bifurcation. Part II – Laser-Doppler anemometer measurements. Journal of Biomechanics. 15**:** 363-378.

Castello, R., Vaughn, M., Dressier, FA., McBride, LR., Willman, VL., Kaiser, G C., Schweiss, JF., Oflli, EO. and Labovitz, AJ. 1995. Relation between pulmonary venous flow and pulmonary wedge pressure: Influence of cardiac output. American Heart Journal.130 (1): 127-134.

Clementel, IEV., Figueroa, CA., Jansen, KE. and Taylor, CA. 2006. Outflow boundary conditions for three-dimensional finite element modeling of blood flow and pressure in arteries. Computer Methods in Applied Mechanics and Engineering. 195: 3776-3796.

Eicke, BM., Schlichting, JV., Mohr-Kahaly, S., Schlosser, A., Bardeleben, RSV., Krummenauer, F. and Hopf, HC. 2001. Lack of Association Between Carotid Artery Volume Blood Flow and Cardiac Output. Journal of Ultrasound and Medicine. 20: 1293-1298.

Formaggia, L., Gerbeau, JF., Nobile, F. and Quarteroni, A. 2001. On the coupling of 3D and 1D Navier-Stokes equations for flow problems in compliant vessels. Computer Methods in Applied Mechanics and Engineering. 191: 561-582.

Ku, DN. and Giddens, DP. 1987. Laser Doppler anemometer measurements of pulsatile flow in a model carotid bifurcation. Journal of Biomechanics. 20: 407–421.

Ku, DN. 1997. Blood flow in arteries. Annual Review of Fluid Mechanics. 29: 399-434.

Liepsch, D. *et al*. 1992. Some flow visualization and Laser-Doppler-velocity measurements in a true to scale elastic model of a human aortic arch-A new model technique. Biorheology. 29: 563-580.

Liepsch, D. and Zimmer, R. 1995. The dynamics of pulsatile flow in distensible model arteries. Technology and Health Care. 3: 185-199.

Marshall, I., Zhao, SZ., Papathanasopoulou, P., Hoskins, P. and Xu, XY. 2004. MRI and CFD studies of pulsatile flow in healthy and stenosed carotid bifurcation models. Journal of Biomechanics. 37: 679-687.

Maurits, NM., Loots, GE. and Veldman, AEP. 2007. The influence of vessel wall elasticity and peripheral resistance on the carotid artery flow wave form: A CFD model compared to in vivo ultrasound measurements. Journal of Biomechanics. 40 (2): 427-436.

Perktold, K. and Hilbert, D. 1985. Numerical simulation of pulsatile flow in a carotid artery bifurcation model. Journal of Biomedical Engineering. 8**:** 193-198.

Perktold, K., Thurner, E. and Kenner, TH. 1994. Flow and Stress Characteristics in Rigid walled and Compliant Carotid Artery Bifurcation Models. Medical and Biological Engineering and Computing. 32: 19-26.

Quarteroni, A., Tuveri, M. and Vencziani, A. 2000. Computational vascular fluid dynamics: problem, models and methods. Computing and Visualization in Science. 2: 163-197.

Rindt, CCM., Steenhoven, AAV., Janssen, JD., Reneman, RS. and Segal, A. 1990. A Numerical Analysis of Steady flow in a Three Dimensional Model of the Carotid Artery Bifurcation. Journal of Biomechanics. 23 (5): 461-473.

Stevens, SA., Lakin, WD. and Goetz, W. 2003. A differentiable, periodic function for pulsatile cardiac output based on heart rate and stroke volume. Mathematical Biosciences. 182: 201–211.

Stroud, JS., Berger, SA. and Saloner, D. 2002. Numerical Analysis of flow through a Severely Stenotic Carotid Artery Bifurcation. Journal of Biomechanical Engineering. Transactions of ASME. 124: 9-20.

Urquiza, SA., Blanco, PJ., Venere, MJ. and Feijoo, RA. 2006. Multidimensional modeling for the carotid artery blood flow. Computer Methods in Applied Mechanics and Engineering. 195 (33-36): 4002-4017.

Van de Vosse, FN., Steehoven, AA. V., Janssen, JD. and Reneman, RS. 1990. A two-dimensional numerical analysis of unsteady flow in the carotid artery bifurcation. Biorheology. 27: 163-189.

Zhao, SZ., Xu, XY., Hughes, AD., Thom, SA., Stanton, AV., Ariff, B. and Long, Q. 2000. Blood flow and vessel mechanics in a physiologically realistic model of a human carotid arterial bifurcation. Journal of Biomechanics. 33: 975-984.